Universal Image Segmentation Framework on High-resolution Automotive Radar Map

Yang Xiao, Scott Cassidy, Liam Daniel, Sukhjit Pooni, Mikhail Cherniakov, Marina Gashinova*

Microwave Integrated Systems Laboratory (MISL), The University of Birmingham, UK
**yxx752@student.bham.ac.uk*

Keywords: Doppler beam sharpening, image segmentation, high-resolution automotive radar map, autonomous driving, multi-variate Gaussian distribution.

Abstract

A universal image segmentation framework, which can be applied to various high-resolution automotive radar imagery produced by different beamforming strategies, is expected in the radar community to provide robust support to the development of autonomous driving. This paper estimates the universality of the segmentation framework, which is developed based on radar data produced by the mechanical steer beamforming, by directly implementing it onto another high-resolution radar imagery produced by the beamforming strategy of MIMO Doppler beam sharpening (DBS). The comparison of the distribution features of two parts of data shows that the return power level shift caused by the resolution difference is the major factor that needs to be compensated for the framework transfer implementation. The details of the universal segmentation framework are given to show that this can significantly simplify the complicated manual labelling and feature extraction. The segmentation results are discussed with the analysis of the performance and the potential future work.

1 Introduction

The next generation of cars with the highest levels of automation requires the combination of multi-modal sensors to perceive the surrounding of the vehicle [1]. The common sensors utilized for modern vehicles include automotive radar, LiDAR, camera, and ultrasonic sensors. Compared with the other sensors, automotive radar is considered as the most reliable sensor robust to harsh weather and bad light conditions [2]. The development of mm-wave and low-THz radar enables the availability of high-resolution automotive radar imagery which provides the full scene representation of the driving environment as an alternative to that based purely on optical imagery [3-5]. Therefore, achieving the full scene reconstruction based on the automotive radar map can provide the key information of the passable and impassable regions to the path planning in autonomous driving.

Learned from the methods developed on optical imagery, radar image segmentation is the solution to identify the passable path purely based on radar information. To do this we need a customized and universal approach that fit the format of radar data and can be extended to various high-resolution automotive radar imagery produced by different beamforming strategies.

The radar segmentation framework is proposed for the first time in our previous publication of [6], which includes the supervised multivariate Gaussian distribution (MGD) region classification based on the distribution features of radar data. The segmentation framework with the MGD classifier has been established, validated, and tested on the radar imagery collected by mechanically steering FMCW radar (PolaRAD-79) operating at 79 GHz to understand the feasibility of segmentation on automotive radar imagery.

In this paper, we study the universality of the developed framework by estimating the feasibility of directly applying it to another high-resolution automotive radar map produced by a different beamforming approach. The new data is collected by MIMO automotive radar with further Doppler beam sharpening (DBS) process to mitigate the side-lobe effects and improve the imaging resolution [7]. We analysed the difference in feature space of two types of high-resolution radar imagery - PolaRAD-79 data and MIMO-DBS data to understand the possibility of directly delivering the region classification without additional data labelling. The estimation and segmentation results showed that the framework produced based on the features of PolaRAD-79 data can be directly utilized for the segmentation of MIMO-DBS data which only requires the translational shift of return power levels at the input of the classifier according to the difference between radar systems. This conclusion is valuable for the automotive radar community since the universal method can be extended to the segmentation of other high-resolution automotive radar imagery without any complicated manual labelling and feature extraction processing.

2 Datasets – PolaRAD-79 and MIMO-DBS

The two high-resolution automotive radar image datasets - PolaRAD-79 and MIMO-DBS were used in this work. The former is produced by the setup shown in Fig. 1 (a), which includes the mechanically steering FMCW radar. The latter is collected by INRAS Radarlog [8] with 4Tx-16Rx MIMO frontend by the platform given in Fig. 1 (b). The set-up which included, both sensor suits included ZED stereo camera,

LiDAR, and, in the case of INRAS data collection, the inertial measurement unit (IMU) utilized for estimating the real-time velocity of the vehicle platform. Parameters of the two radar systems are listed in Table 1.

Table 1. The characteristic parameters of radar systems.

Parameter	INRAS Radarlog	PolaRAD-79
Bandwidth	1 GHz	5 GHz
Start frequency	76 GHz	76 GHz
Mode of operation	MIMO	Mechanical steer FMCW
Tx antenna gain	14.4 dBi	30 dBi
Rx antenna gain	14.4 dBi	30 dBi
Transmit power	10 dBm	13 dBm
Range resolution	15 cm	3 cm

All the details of the formation of the PolaRAD-79 dataset are given in [6], which includes the raw data collection, the pre-processing by conducting free space loss calibration, and the manual labelling procedure of radar image frames.

The MIMO-DBS automotive radar map is developed in [7]. Automotive radars typically use MIMO beamforming to resolve the angular position of targets, and the resolution is limited by the number and configuration of transmitting and receiving elements [9]. DBS is the synthetic technique to produce the independent estimation of the target angular position [10] based on the platform movement. The strategy of DBS is to refine the antenna beam into narrow sub-beams. The sub-beams are split by different Doppler shifts caused by the radial velocity change under various azimuth angles. The resolution of radar imaging can therefore be improved by implementing narrowband filters on individual sub-beam through the whole beam pattern.

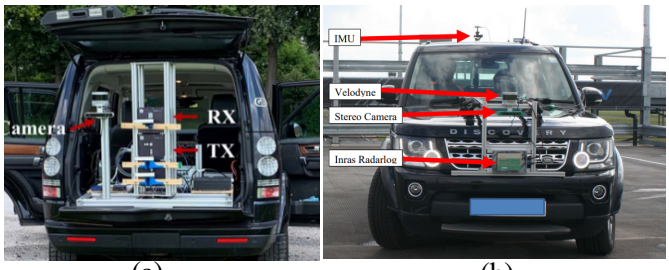

(a) (b)

Fig. 1 (a) The platform for collecting the PolaRAD-79 dataset. (b) The platform for collecting the MIMO-DBS dataset.

When combined MIMO-DBS is able to improve angular resolution and decrease inherent MIMO side-lobe levels [7]. Based on the MIMO radar map which is produced by performing two-dimensional FFT on the single MIMO frame, another Doppler FFT is performed in slow time by assembling N frames of radar maps to obtain the Doppler map. Samples are extracted where MIMO and DBS derived angles overlap, to produce a single range-angle map with significantly improved resolution and reduced side-lobe levels as shown in Fig. 2.

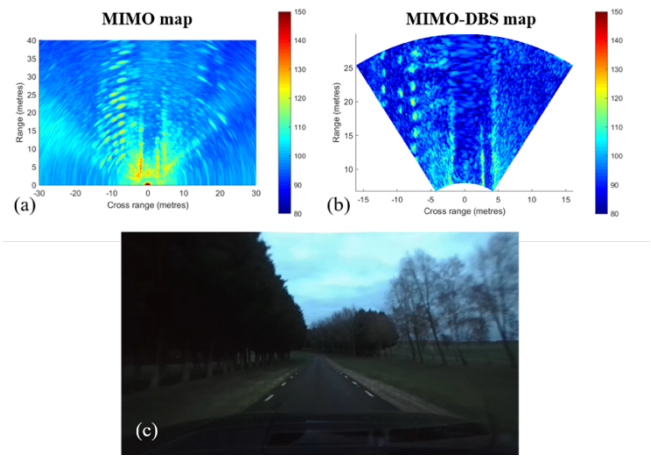

Fig. 2 (a) The original MIMO map; (b) the radar map after implementation of DBS on (a); (c) the corresponding optical imagery.

As can be seen from this figure such improvement results in excellent contrast between different regions within the map (trees, curb, grassy roadside) which is the necessary pre-requisite of image segmentation.

3 Distribution Feature Analysis

The segmentation process includes the pre-segmentation stage using Canny-edge detection, and the region classification using MGD classifier as described in [6]. The physical features of returns from different terrain types and objects are based on the shape and scale factor of their Weibull PDF and are used as the input of the MGD classifier. Importantly choice of Weibull distribution is based not on the best fit, but on one which can produce better contrast between different classes of terrain and objects [6]. Therefore, to validate the transferability of the developed image segmentation approach, the Weibull distribution feature parameters were extracted and compared for both data types – PolaRAD-79 and MIMO-DBS. The classes are grass, objects, asphalt, and shadows chosen as a required minimum for the path planning.

The Weibull distribution feature parameters obtained from the PolaRAD-79 dataset in different range groups are shown in Fig. 3 [6] as the comparison baseline. The feature parameters are obtained by fitting Weibull distribution on the density histogram of calibrated and uncalibrated radar data of manually labelled regions corresponding to chosen classes. The data calibration here means the return power whitening over ranges according to the free space loss model as described in [6].

Weibull distribution parameters obtained from the new MIMO-DBS dataset is shown in Fig. 4. The return power calibration is based on the same free space loss model in [6], and the manual labelling of regions on MIMO-DBS maps was only used for this analysis.

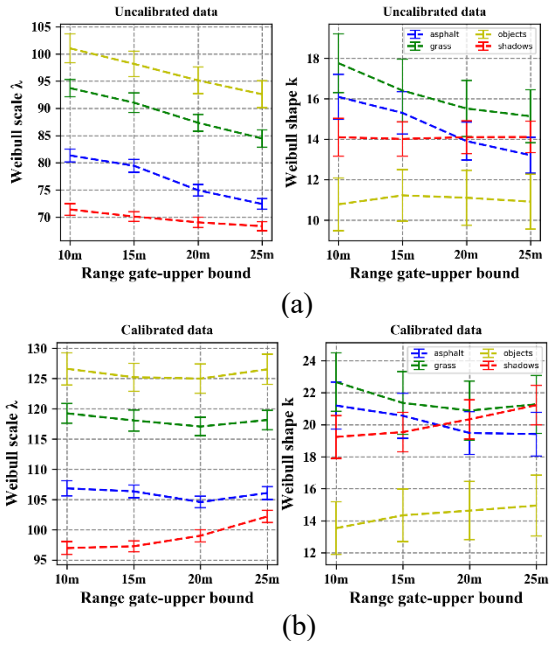

Fig. 3 The Weibull distribution parameters from PolaRAD-79 dataset [6].

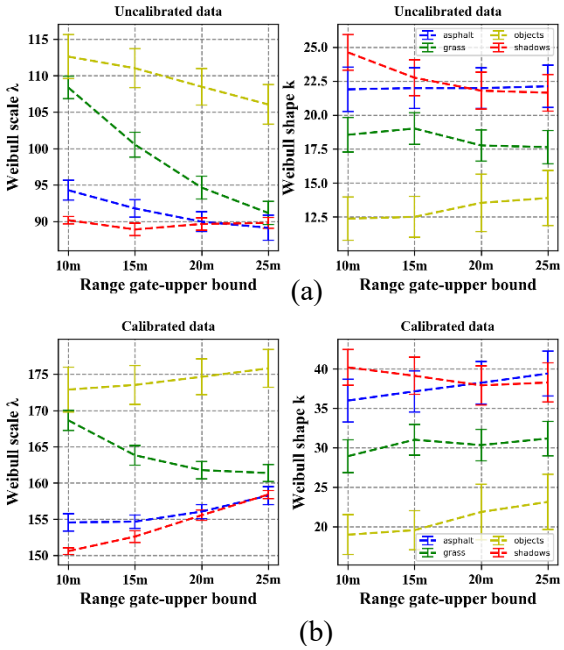

Fig. 4 The Weibull distribution parameters from MIMO-DBS radar maps.

Comparing Fig. 3 and 4 we can draw the following conclusions:
1) For both datasets parameters of classes of objects, grass, and asphalt demonstrate a clear contrast.
2) Both λ and k parameters of asphalt and shadows show slight differences within the range of 15 m, and merge at longer ranges. This can be explained as the lower transmitted power and antenna gains of the INRAS Radarlog system than PoloRAD-79 system will lead to the shorter range to resolve returns from the asphalt above the noise floor [11].

3) The Weibull scale parameter λ of MIMO-DBS is higher than PolaRAD-79, which is similar to Weibull shape k parameters:

$$f(x;\lambda,k)=\begin{cases}\frac{k}{\lambda}\left(\frac{x}{\lambda}\right)^{k-1}e^{-\left(\frac{x}{\lambda}\right)^{k}}, & x\geq 0\\ 0, & x<0\end{cases} \quad (1)$$

here x is the input variable.

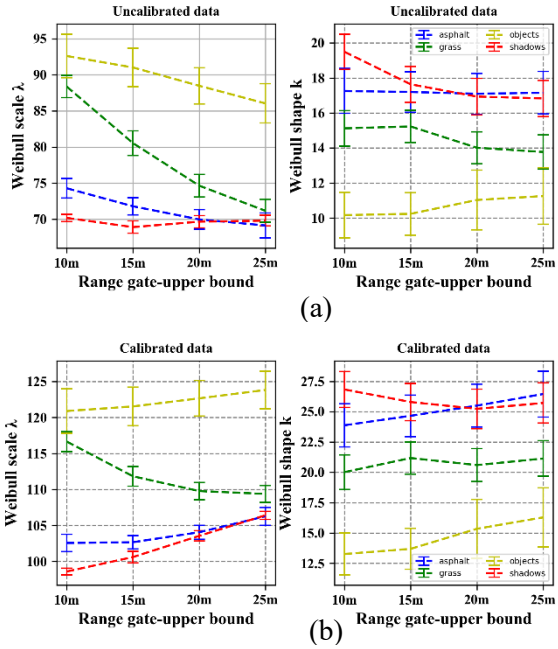

Fig. 5 The Weibull distribution feature parameters of MIMO-DBS maps after return power shift.

If the distribution of return power is only scaled for two datasets, the initial ratio factor of $\frac{k}{\lambda}$ need to be constant which indicates that k will shift along with λ. Under this assumption, we conduct the following parameter shift according to the average power level difference between two radar systems. The shifted λ parameter of MIMO-DBS is calculated as:

$$\lambda'_{DBS}=\lambda_{DBS}-a \quad (2)$$

where a is the average power level difference between two radar systems and λ_{DBS} is the original Weibull scale parameter. We would like to stress that a can be determined as the power level difference of the specific area class such as "objects", or it can be more robustly obtained by searching through a range of values to find out the power shift value which can give the best segmentation performance. The shifted k parameter can therefore be calculated as:

$$k'_{DBS}=\left(\frac{k_{DBS}}{\lambda_{DBS}}\right)*(\lambda_{DBS}-a) \quad (3)$$

where k_{DBS} is the original Weibull shape parameter.

The shifted feature parameters are plotted in Fig. 5, which approach the feature parameters shown in Fig. 3 as expected. This estimation indicates that the region classification model

established based on the PolaRAD-79 data can be directly utilized for the MIMO-DBS maps by simple compensation on the power level difference. The implementation details will be discussed next.

4 Universal Image Segmentation Framework

According to the analysis in the previous section, we can conclude that the MGD classifier is universal to multiple types of high-resolution automotive radar maps with return power distribution scaling in the pre-processing stage. Therefore, the MGD classifier trained using labelled dataset on one radar beamformer can be applied directly to the other without the necessity to repeat manual labelling and training on another dataset.

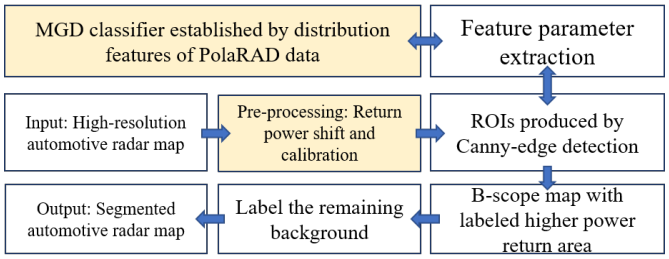

Fig. 6 The block diagram of the universal image segmentation framework.

The block diagram of the image segmentation framework is shown in Fig. 6. The test automotive radar map is the input of the framework, and the segmented radar map is obtained at the output. There are two steps related to the distribution feature representation of radar data which are the pre-processing and the MGD region classification.

The pre-processing stage requires parameters scaling by Eq. (2) and (3), after the radar data calibration to compensate for return power difference according to the range. This is done by applying the polynomial range-dependant factor to the range profiles within the imagery [6]:

$$f_c = -5.7 \times 10^{-6} R^4 + 0.001 R^3 - 0.05 R^2 + 0.36 R - 26.4 \quad (4)$$

where R is the range.

After the pre-processing, the extracted parameters, considered as the input features of classifiers of the test data, are expected to produce the contrast position in feature space. The feature difference between the dataset used for initial supervised training, the PolaRAD-79, and the dataset of MIMO-DBS are shown in Fig. 7. The color-coded background in Fig. 7 (a) and (b) are the surface plot of the pdfs of 2-dimensional MGD classifier calculated by the Weibull scale and shape parameters of PolaRAD-79 (Fig 7 (a)) and scaled MIMO-DBS data (Fig 7 (b)) Two circled areas contoured by blue and black represent the distribution peaks of area classes of grass and objects, shown as yellow and green dots. The distribution of scattered feature points from both dataset approaches to the MGD peaks of the corresponding area class. This indicates that the MGD classifier given here can accurately describe the distribution of the features obtained from various data formats.

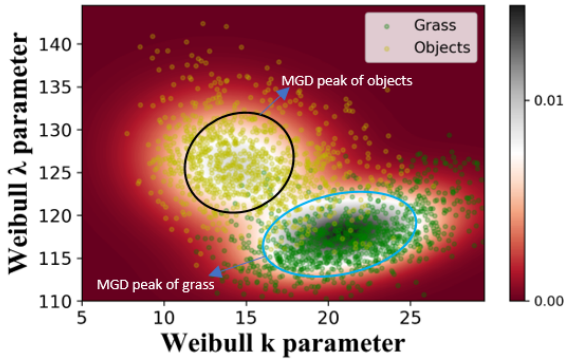

(a)

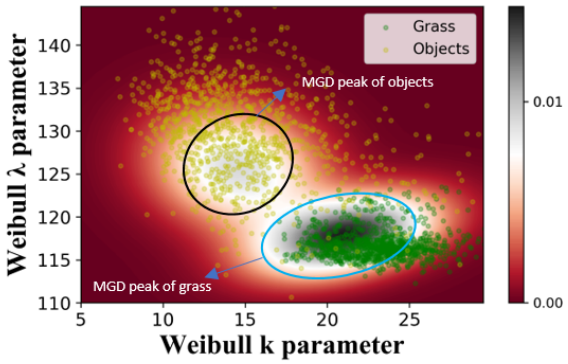

(b)

Fig. 7 (a) The PDF of MGD classifier and the parameters obtained from PolaRAD-79 data; (b) The PDF of MGD classifier of PolaRAD-79 data and the parameters obtained from MIMO-DBS data.

The dimension of the MGD model depends on the number of the input feature parameters. The MGD model utilized in our proposed segmentation framework is four-dimensional with the input feature parameters of:

$$x_t = [k_w^{un}, \lambda_w^{un}, k_w^c, \lambda_w^c] \quad (5)$$

where k_w^{un}, λ_w^{un} are the Weibull shape and scale parameters of the uncalibrated data, and k_w^c, λ_w^c are parameters of the calibrated data. The general pdf definition of the n-dimensional MGD model is:

$$\mathrm{p}(x_t) = \frac{1}{(2n)^{\frac{n}{2}} |\Sigma|^{\frac{1}{2}}} e^{-\frac{1}{2}(x_t - M)^T \Sigma^{-1} (x_t - M)} \quad (6)$$

where for our case n = 4. Σ is the covariance matrix, and M is the vector of the mean values of feature parameters which are different for different classes.

For the grass and objects areas, the covariance matrices of Σ_{grass} and $\Sigma_{objects}$ are:

$$\Sigma_{grass} = \begin{vmatrix} 9.1 & 8.8 & 11.5 & 8.1 \\ 8.8 & 19 & 9.3 & 12.6 \\ 11.5 & 9.3 & 15.3 & 10.8 \\ 8.1 & 12.6 & 10.8 & 16 \end{vmatrix} \quad (7)$$

$$\Sigma_{objects} = \begin{vmatrix} 8.9 & -1.2 & 12 & -1 \\ -1.2 & 32 & -4.1 & 21.6 \\ 12 & -4.1 & 16.3 & -2.3 \\ -1 & 21.6 & -2.3 & 20.4 \end{vmatrix} \quad (8)$$

The mean value vectors of feature parameters are:

$$M_{grass} = [16.6, 87.8, 22.3, 117.6] \quad (9)$$

$$M_{objects} = [11.9, 96.6, 15.7, 126.5] \quad (10)$$

The MGD classifiers of areas of grass and objects are calculated using the above parameters, and the region classification of the other high-resolution radar maps can be achieved by inputting the feature parameters in the same order as Eq. (5).

5 Segmentation Results on MIMO-DBS Maps

The results of segmentation based on MGD classifier trained on PolaRAD-79 data and applied to scale MIMO-DBS data area shown in Fig. 8 and 9.

The optical imagery, the MIMO-DBS automotive radar map, and the segmented maps showed that segmentation results correspond to the ground truth and that the drivable areas are correctly bounded by impassable regions of grass and object.

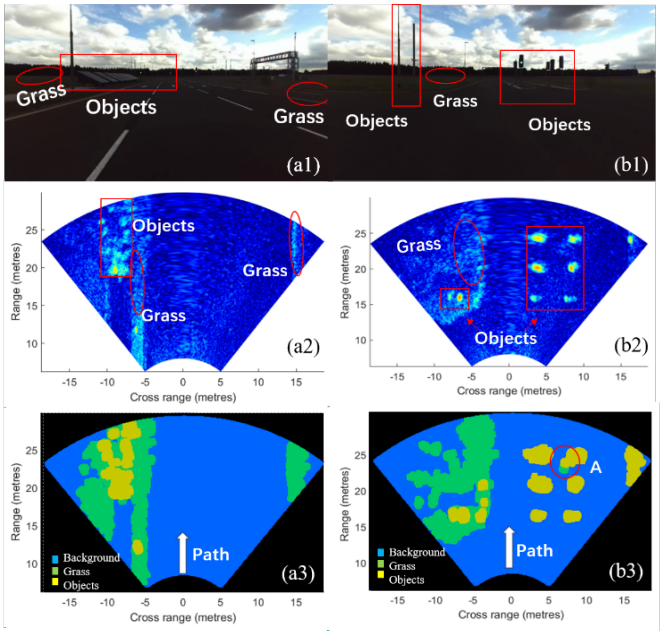

Fig. 8 (a1)-(b1) are the photos of the open road scene; (a2)-(b2) are corresponding MIMO-DBS radar maps; (a3)-(b3) are segmented MIMO-DBS maps.

Some of the confusions between grass and objects are observed: 1) the region of A in Fig. 8 (b3) and the region of D in Fig. 9 (b3) are wrongly identified as grass due to the over-segmentation in pre-segmentation. This can be improved by optimizing the pre-segmentation and using frame-to-frame tracking of regions; 2) the region of B in Fig. 9 (a3) is identified as the class 'object' due to the fact that narrow gravel roadside alongside the road produces a higher power return due to the rougher surface than grass area. This problem can be addressed by increasing the number of classes in the future.

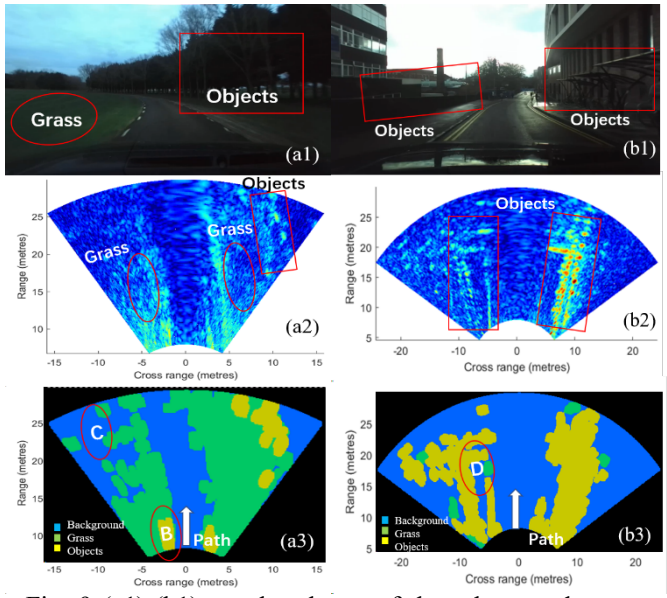

Fig. 9 (a1)-(b1) are the photos of the urban road scene; (a2)-(b2) are corresponding MIMO-DBS radar maps; (a3)-(b3) are segmented MIMO-DBS

Region C in Fig. 9 (a3) is not correctly identified in the segmentation is due to the deviation of velocity estimation between the left and right sides used for DBS. This will be improved by involving the velocity compensation in the DBS procedure when the vehicle is cornering.

6 Conclusions

In this paper, we present the universal segmentation framework for high-resolution automotive radar imagery which includes the MGD region classification based on the distribution parameter features. The universality is estimated and discussed from two aspects: 1) the analysis of the distribution features of different high-resolution radar imagery; 2) the feasibility of implementing the framework developed based on the PolaRAD-79 data on the MIMO-DBS maps. Both feature analysis and segmentation results showed that the transfer of the segmentation framework is possible between differently generated high-resolution automotive radar imagery by simply scaling the return power. It is shown that MGD based classifier based on the manually labelled training dataset obtained for one radar, can successfully be applied to another radar data without the necessity to repeat the tedious labelling process.

7 Acknowledgements

This work is supported by Innovate UK grant 104268 and is part of the project "CORTEX-Cognitive Real-Time System for Autonomous Vehicles".

8 References

[1] F. Duarte and C. Ratti, "The impact of autonomous vehicles on cities: A review," *Journal of Urban Technology,* vol. 25, no. 4, pp. 3-18, 2018.

[2] L. Daniel, D. Phippen, E. Hoare, A. Stove, M. Cherniakov, and M. Gashinova, "Low-THz radar, lidar and optical imaging through artificially generated fog," 2017.

[3] Y. Xiao, F. Norouzian, E. G. Hoare, E. Marchetti, M. Gashinova, and M. Cherniakov, "Modeling and experiment verification of transmissivity of low-THz radar signal through vehicle infrastructure," *IEEE Sensors Journal,* vol. 20, no. 15, pp. 8483-8496, 2020.

[4] D. Jasteh, M. Gashinova, E. Hoare, T.-Y. Tran, N. Clarke, and M. Cherniakov, "Low-THz imaging radar for outdoor applications," in *2015 16th International Radar Symposium (IRS)*, 2015: IEEE, pp. 203-208.

[5] F. Norouzian, E. Hoare, E. Marchetti, M. Cherniakov, and M. Gashinova, "Next generation, Low-THz automotive radar–the potential for frequencies above 100 GHz," in *2019 20th International Radar Symposium (IRS)*, 2019: IEEE, pp. 1-7.

[6] Y. Xiao, L. Daniel, and M. Gashinova, "Image segmentation and region classification in automotive high-resolution radar imagery," *IEEE Sensors Journal,* vol. 21, no. 5, pp. 6698-6711, 2020.

[7] S. Cassidy, S. Pooni, M. Cherniakov, E. Hoare, and M. Gashinova, "High resolution automotive imaging using MIMO radar and Doppler beam sharpening," *Submitted to IEEE Transactions on Aerospace and Electronic Systems*.

[8] "Inras Radarlog." https://inras.at/en/radarlog/ (accessed 05/05/2022.

[9] J. Li and P. Stoica, *MIMO radar signal processing*. John Wiley & Sons, 2008.

[10] L. Daniel *et al.*, "Application of Doppler beam sharpening for azimuth refinement in prospective low-THz automotive radars," *IET Radar, Sonar & Navigation,* vol. 12, no. 10, pp. 1121-1130, 2018.

[11] Y. Xiao, L. Daniel, and M. Gashinova, "The End-to-End Segmentation on Automotive Radar Imagery with MTI based on Frame-to-Frame Association," *In progress, intend to be submitted to IEEE Sensors Journal,* 2022.